Local Ordering in the Intermetallic Compound $Cu_{1-x}Al_2$ Studied by NMR Spectroscopy

Frank Haarmann,* Marc Armbrüster, and Yuri Grin

Max-Planck-Institut für Chemische Physik fester Stoffe, Nöthnitzer Str. 40, 01187 Dresden, Germany

Received September 27, 2006. Revised Manuscript Received December 5, 2006

The relation between the homogeneity range and the chemical bonding in the intermetallic compound $Cu_{1-x}Al_2$ was investigated by nuclear magnetic resonance spectroscopy. $^{63,65}Cu$ and ^{27}Al NMR spectroscopy experiments were carried out on Al- and Cu-rich powder samples of the binary phase $Cu_{1-x}Al_2$. Solely combined application of several NMR techniques like orientational dependent measurements of powder samples aligned in a magnetic field and spin echo double resonance (SEDOR) experiments revealed the formation of vacancies at the copper sites. Two other possible mechanisms substitution of Cu by Al and vice versa, were excluded.

1. Introduction

Non-stoichiometric composition of matter is often observed and has a significant impact on the properties in solid state, especially in intermetallic compounds. The understanding of properties of these compounds is strongly related to the understanding of chemical bonding. The intermetallic phase $Cu_{1-x}Al_2$ is relevant in the hardening process of aluminum alloys.[1−3] Since the material is of significant importance for the industry the binary system Cu−Al belongs to the best investigated ones. The formation conditions for the phases are well-known,[1,4−10] and a comprehensive review of the phase diagram is given by Murray.[11] The existence of the homogeneity range of $Cu_{1-x}Al_2$ was found first in ref 10 and was later confirmed to be $0.012 \leq x \leq 0.059$ at 500 °C.[12] Interestingly, increasing copper deficiency corresponds to an increase of the lattice parameters.[12,13]

The crystal structure of $Cu_{1-x}Al_2$ was analyzed for the first time by X-ray film data.[14] Detailed reinvestigations based on single-crystal X-ray diffraction data confirmed the primary model with one crystallographic position for the Cu atoms and one for the Al atoms.[12,15] No direct evidence for defects on the Cu site was found from single-crystal structure determination, though the ratio $B_{iso}(Cu)/B_{iso}(Al) \approx 0.83$ in both publications[12,15] seems to be too large compared to the expected value of 0.65 from the atomic masses. This finding is an indicator for defects on the copper position.

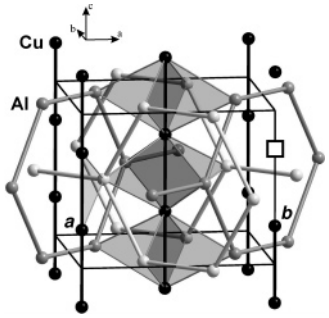

Figure 1. Crystal structure of and chemical bonding in $Cu_{1-x}Al_2$. A Cu vacancy is marked by a square. Cu sites owing a different environment are marked by *a* and *b*. Covalently bonded interpenetrating aluminum nets are shown with gray Al−Al bonds. The triangles visualize three-center bonds, Cu−Al−Cu.

$Cu_{1-x}Al_2$ may serve as a prototype material for the study of non-stoichiometric intermetallic phases because of the good knowledge of its chemical bonding situation. A recent analysis of the chemical bonding of $Cu_{1-x}Al_2$ revealed interpenetrating 6^3-nets, formed by covalently three-bonded Al atoms which are interconnected via Cu−Al−Cu three-center bonds[12] (Figure 1). The weaker three-center linking of the copper atoms to the aluminum network permits copper vacancies in the crystal structure.

Various models describing the structural realization of the deviation from the composition 1:2 were discussed in the literature. The occupation of Cu sites by Al (model I) is favored by combined mass density and X-ray diffraction measurements.[13] A model with vacancies at the Cu positions (model II) was rejected in this investigation.

Nuclear magnetic resonance experiments give valuable information of the environments of the atoms either by the signals or more detailed by the internuclear couplings.[16] Two

* Corresponding author.

(1) Guinier, A. *Nature* **1938**, *142*, 569.
(2) Wassermann, G.; Weerts, J. *Metallwirtschaft* **1935**, *14*, 605.
(3) Eshelman, F. R.; Smith, J. F. *J. Appl. Phys.* **1978**, *49*, 3284.
(4) Preston, G. D. *Nature* **1938**, *142*, 570.
(5) Preston, G. D. *Proc. R. Soc. London, Ser. A* **1938**, *167*, 526.
(6) Preston, G. D. *Philos. Mag.* **1938**, *26*, 855.
(7) Silcock, J. M.; Hardy, T. J. *J. Inst. Met.* **1953**, *82*, 239.
(8) Kelly, A.; Nicholson, R. B. *Prog. Mater. Sci.* **1945**, *33*, 1957.
(9) Stockdale, D. *J. Inst. Met.* **1933**, *52*, 111.
(10) Gödecke, T.; Sommer, F. *Z. Metallkd.* **1996**, *87*, 581.
(11) Murray, J. K. *Int. Met. Rev.* **1985**, *30*, 211.
(12) Grin, Y.; Wagner, F. R.; Armbrüster, M.; Kohout, M.; Leithe-Jasper, A.; Schwarz, U.; Weding, U.; von Schnering, H. G. *J. Solid State Chem.* **2006**, *179*, 1707.
(13) Zogg, H. *J. Appl. Crystallogr.* **1979**, *12*, 91.
(14) Friauf, B. *J. Am. Chem. Soc.* **1927**, *49*, 3107.
(15) Meetsma, A.; De Boer, J. L.; Van Smaalen, S. *J. Solid State Chem.* **1989**, *82*, 370.
(16) Laws, D. D.; Bitter, H.-M.; Jerschow, A. *Angew. Chem.* **2002**, *114*, 3224.

10.1021/cm062313k CCC: $37.00
Published on Web 02/08/2007

earlier NMR investigations, focusing only on the line shapes of the signals, report a second resonance for Cu in $Cu_{1-x}Al_2$. Yamaguchi et al.[17] attributed the second resonance to a metastable phase and Bastow and Celotto[18] assigned it to a so-called *anti-side* order, where Cu atoms are placed on the Al sites (model III). This copper-rich model is in contradiction to the chemical composition and, furthermore, appears unlikely with respect to chemical bonding.[12]

In the present work we investigate the structural realization of the homogeneity range of $Cu_{1-x}Al_2$ by wide-line NMR experiments. From the analysis of the internuclear couplings determined on a sample of $Cu_{1-x}Al_2$ aligned in a magnetic field we aim to develop an unambiguous model describing the local order of the atoms. Along this line an agreement with the chemical bonding analysis is achieved, and an explanation for the lattice expansion with decreasing Cu content will be given.

2. Experimental Section

2.1. Samples. An aluminum-rich single crystal of $Cu_{1-x}Al_2$ of about 2 cm^3 volume was used as starting material for samples 1−4. The single crystal with the composition $Cu_{0.975(8)}Al_2$ was characterized by X-ray diffraction, metallographic investigations, chemical analysis, and WDXS analysis. Further details of the preparation of the single crystal and its characterization are described in refs 12 and 19.

A polycrystalline Cu-rich two-phase sample 5 ($Cu_{1-x}Al_2$ with traces of CuAl) of nominal composition $CuAl_2$ was synthesized by melting the elements (Cu 99.9% and 99.999% Al, both ChemPur) in an arc melter (model 5BJ, Centor Vacuum Industries). Subsequent thermal annealing was performed in evacuated quartz glass ampules at 400 °C for 14 weeks.

As a result of the extremely reduced NMR signal intensity caused by the small penetration depth of electromagnetic radiation in materials with metallic conductivity (so-called skin effect), the single crystal had to be pulverized for the NMR experiments. After crushing in a mortar the sample was additionally treated in a planetary micromill (Pulverisette 7, Fritsch). A fraction of powder with a particle size between 25 μm and 50 μm was used for the NMR measurements.

The possible influence of the mechanical treatment on the NMR signals of $Cu_{1-x}Al_2$ was investigated on samples annealed at 400 °C being sealed in evacuated quartz glass tubes (0 h for sample 1, 24 h for sample 2, 4 months for sample 3).

Magnetic alignment of the crystallites was achieved by slow hardening of a suspension of sample 2 in two-component glue (UHU endfest 300) in an external magnetic field of 11.74 T (sample 4).

The polycrystalline sample 5 was crushed in a mortar and sieved to obtain a particle size between 25 μm and 50 μm. The selected powder was annealed for 24 h at 400 °C in evacuated quartz glass ampules prior to the NMR measurements.

2.2. Sample Characterization. X-ray powder diffraction was carried out on a Huber image plate camera G670 in transmission geometry applying Cu Kα_1 radiation (λ = 1.540562 Å, Ge monochromator) in a 2θ range from 15° to 85°. The X-ray powder diffraction pattern of the milled samples 1−3 did not reveal any impurities besides SiAlON which is due to abrasion during the milling (Figure 2).

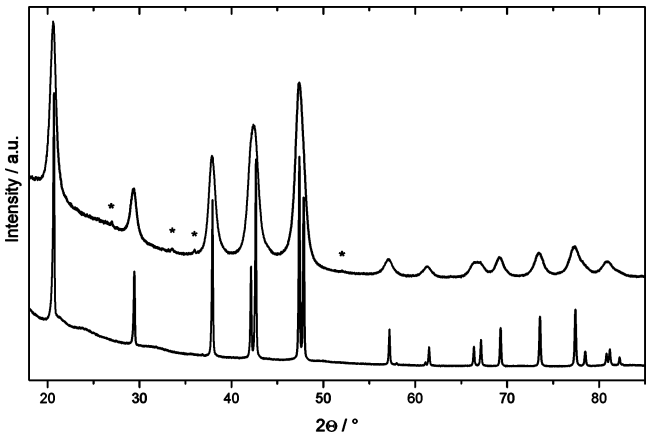

Figure 2. X-ray powder diffraction patterns: Al-rich $Cu_{1-x}Al_2$ (bottom); the same sample after milling (top). The asterisks mark SiAlON-peaks due to abrasion in the micromill. The massive increase in the full width at half-maximum shows the stress in the crystal structure due to the milling process.

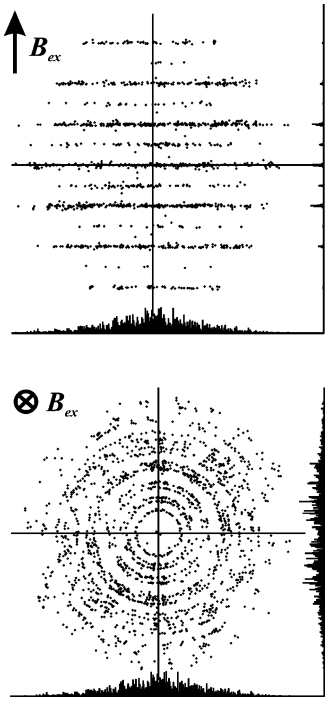

Figure 3. X-ray diffraction pattern of the sample $Cu_{1-x}Al_2$ aligned in a magnetic field (sample 4) perpendicular (top) and parallel to [001] (bottom). The *c* axis of the crystallites is aligned parallel to the orienting magnetic field B_{ex}, while perpendicular to the field direction no preferred orientation of the *a* and *b* axes is observed.

A Stoe IPDS setup with Ag Kα radiation (λ = 0.56086 Å, graphite monochromator) was used for X-ray diffraction investigations on sample 4 oriented in the magnetic field. A thin slice perpendicular to the direction of the aligning magnetic field was prepared. All crystallites are aligned with their *c* axes parallel to the orienting field, while perpendicular to the *c* axis no ordering is observed (Figure 3).

2.3. NMR Experiments. The NMR investigations were performed at ambient temperature using a Bruker AVANCE and a Bruker MSL spectrometer with magnetic fields of 11.74 and 7.04 T, respectively. The corresponding frequencies of the ^{63}Cu and the ^{65}Cu isotopes are 132.614 and 142.058 MHz in a magnetic field of

(17) Yamaguchi, S.; Wagatuma, F.; Shinohara, T. *Philos. Mag. Lett.* **1999**, *79*, 171.
(18) Bastow, T. J.; Celotto, S. *Acta Mater.* **2003**, *51*, 4621.
(19) Armbrüster, M. Bindungsmodelle für intermetallische Verbindungen mit der Struktur des $CuAl_2$-Typs. Thesis, Technische Universität Dresden, Dresden, 2004 (Cuvillier Verlag Göttingen, 2005).

11.74 T and 79.618 and 85.288 MHz for 7.04 T, respectively. ^{27}Al NMR experiments were exclusively performed using the 11.74 T field with a corresponding resonance frequency of 130.321 MHz.

A standard 4 mm cross polarization magic angle spinning (MAS) probe was employed with and without sample rotation. As a result of eddy currents, the samples had to be diluted with SiO_2 powder for MAS experiments, which were performed in a ZrO_2 rotor with 4 mm diameter. The samples were filled in quartz glass tubes of 5 mm diameter for all wide-line experiments. These were mounted on low-Q wide-line probes built by Bruker (Karlsruhe, Germany) and NMR-Service (Erfurt, Germany). A wide-line probe designed for double resonance experiments with close frequencies[20] built by NMR-Service (Erfurt, Germany) was utilized for the spin echo double resonance (SEDOR) experiments.[21]

Single-pulse excitation was used for the MAS experiments. For the wide-line measurements an echo sequence with pulses of equal duration was applied. The interpulse distance was optimized to 60 μs to avoid distortions of the signal. For selective excitation experiments low-power pulses with a duration of $\tau(\pi/2) = 100$ μs were used, while for the single wide-line spectra high-intensity pulses of short duration (1.5 μs) were employed. The SEDOR experiments were performed with an interpulse delay of 200 μs and pulse durations of $\tau(\pi/2) = 50$ μs for the **I** spins and $\tau(\pi) = 25$ μs for the **S** spins in heteronuclear ^{65}Cu−^{63}Cu and ^{65}Cu−^{27}Al experiments. All NMR measurements were performed by eightfold cyclization of the pulse sequences.

The interaction of the nuclear quadrupole moment with the electric field gradient is described by the quadrupolar coupling constant defined as $C_Q = e^2qQ/h$ and by the asymmetry parameter $\eta = (V_{xx} - V_{yy})/V_{zz}$.[22] The latter describes the symmetry of the electric field gradient.

Least-square fitting and simulation of the signals was done using the SIMPSON software package.[23] The Cu signals are referenced to a solution of $[Cu(NCMe)_4]ClO_4$ in MeCN, and the Al signal is referenced to a D_2O solution of $Al(NO_3)_3$.

3. Results and Discussion

3.1. Copper NMR.

3.1.1. Line Shape and Parameters of the Spectrum. The X-ray powder diffraction measurements revealed a strong influence of the milling on the crystallinity of the samples (Figure 2). The NMR signals of sample 2 annealed after milling show a sharp second-order perturbed quadrupolar central transition *A* and two additional contributions *B* and *C* (Figure 4). The spectrum of the thermally untreated sample 1 shows in principle the same features, but these are smeared out because of the disorder introduced by the mechanical treatment. The disorder causes small changes in the local environment of the atoms, each accompanied by an individual quadrupolar frequency which results in a distribution of quadrupolar frequencies.[24] The primary annealing obviously reduces the disorder (sample 2). Further annealing of the compound (sample 3) has no influence on the line shape. A continuous decrease of the intensity of contribution *B* with increasing annealing time at 360 °C was observed by Yamaguchi et al.[17] The different annealing behavior indicates the influence of the temperature on the reduction of the disorder.

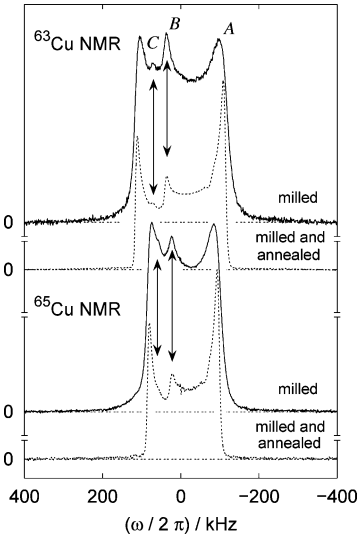

Figure 4. Central transition of the ^{63}Cu and ^{65}Cu NMR signals of Al-rich $Cu_{1-x}Al_2$ samples. Full lines represent spectra of sample 1 after the milling process while dotted lines represent spectra of sample 2 after annealing for 24 h at 400 °C. Additional signal contributions are marked by arrows. The signals are normalized to the same value of maximum intensity, and the frequency range is given relative to the used carrier frequency.

The spectrum of the central transition of the main component *A* is described by an axial symmetric tensor ($\eta = 0$) with coupling constants determined by least-square fitting of $C_Q = 15.2(1)$ MHz and $C_Q = 13.9(1)$ MHz for the ^{63}Cu and the ^{65}Cu isotope, respectively. The observed Knight shift of the main Cu signal is $K = 0.165(5)\%$. This is in agreement with former results.[17,18,25] Thus, this signal can be assigned without doubt to the Cu atoms with regular environment.

The additional contribution *B* was also observed by Yamaguchi et al.[17] and was assigned to a small amount of a metastable phase. Bastow and Celotto[18] detected two additional resonances which were attributed to Cu atoms located at the Al position (model III) and to CuAl as a known impurity in the sample. The frequency of this latter signal does not fit the frequency of contribution *C* being not observed in both investigations[17,18] probably due to the lower signal-to-noise ratios of these studies.

The splitting of the two additional contributions *B* and *C* observed in our experiments is slightly smaller for the ^{65}Cu than for the ^{63}Cu isotope. This indicates quadrupole coupling as origin of the splitting, because chemical shielding or Knight shift would increase the splitting from ^{63}Cu to the ^{65}Cu resonance. Therefore, contributions *B* and *C* orginate most probably from the second-order splitting of a signal belonging to only one additional type of Cu atoms.

An estimation of the amount of the additional signal cannot be given without additional knowledge concerning its corresponding quadrupole coupling tensor. However, the influence of the Cu content on the intensity of the additional signal is small. No significant change of the intensity ratio was observed for the Cu-rich two-phase sample 5.

(20) Haase, J.; Curro, N. J.; Slichter, C. P. *J. Magn. Reson.* **1998**, *135*, 273.
(21) Emshwiller, M.; Hahn, E. L.; Kaplan, D. *Phys. Rev.* **1960**, *118*, 414.
(22) Slichter, C. P. *Principles of Magnetic Resonance*, 3rd ed.; Springer-Verlag: Berlin, 1990.
(23) Bak, M.; Rasmussen, J. T.; Nielsen, N. C. *J. Magn. Reson.* **2000**, *147*, 296.
(24) Mehring, M.; Kanert, O. *Z. Naturforsch.* **1969**, *24A*, 332.
(25) Torgeson, D. R.; Barnes, R. G. *J. Chem. Phys.* **1975**, *62*, 3968.

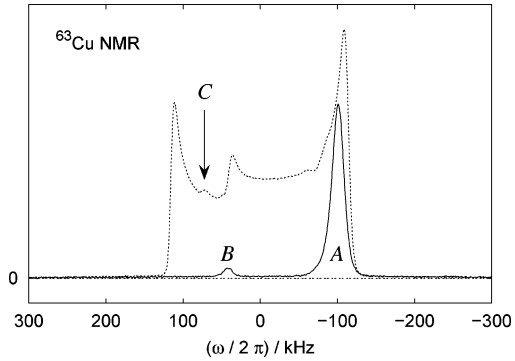

Figure 5. Central transition of the ^{63}Cu NMR signals of $Cu_{1-x}Al_2$, non-oriented sample 2 (dotted line), and sample 4 aligned in a magnetic field (solid line). The angle between the orienting and the external magnetic field B_0 of the measurement is $\theta \approx 45°$. The signals of the main (*A*) and the minor (*B*) components are observed in both samples. The position of contribution *C* in the non-oriented sample 2 is marked by an arrow. For intensities of *C* see text. The intensity of the signals is scaled to prevent overlap, and the frequency scale is given relative to the used carrier frequency.

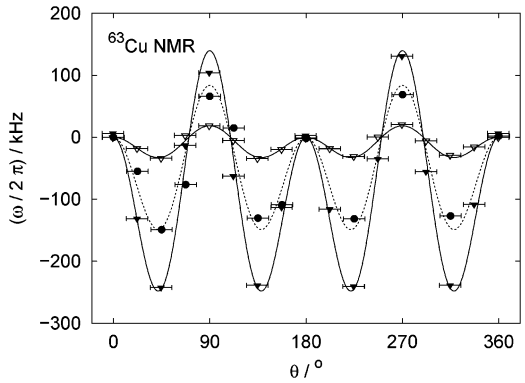

Figure 6. Frequency shift of the ^{63}Cu NMR signals of the Al-rich $Cu_{1-x}Al_2$ sample 4 aligned in a magnetic field in dependence on the orientation with respect to the magnetic fields used for the alignment of the crystallites and for the measurements. Full symbols represent the main signal *A* and open symbols the minor signal *B*. The lines show the calculated frequency shifts for $C_Q = 15.4$ MHz and $C_Q = 5.6$ MHz for magnetic fields of $B_0 = 11.74$ T (dotted line) and $B_0 = 7.04$ T (full lines), respectively.

3.1.2. Orientation-Dependent Measurements. Figure 5 shows the main transition of the ^{63}Cu line shapes of regular powder sample 2 and sample 4 oriented in a magnetic field. The latter reveals the two resolved signals *A* and *B*, with an intensity ratio I_B/I_A of about 1:24 being a proof that both signals are due to bulk atoms.

The variation of the frequency of both ^{63}Cu NMR signals in dependence of the angle (θ) between the orienting and the measurement magnetic field is shown in Figure 6. The frequency dependencies of the signals indicate that both are due to a second-order quadrupolar shift. The change of the frequency of signal *A* with θ is for both magnetic fields in agreement with a quadrupole coupling constant $C_Q = 15.4(1)$ MHz determined by an analysis of the line shape of the main transition. The change of the frequency with θ cannot satisfactorily be resolved for signal *B* in the high field, but a measurement at the lower field of $B_0 = 7.04$ T results in a better resolution. The frequency dependence of signal *B* indicates an almost axial symmetric tensor ($\eta \approx 0$) with a quadrupolar coupling constant of about $C_Q \approx 5.6(2)$ MHz. This clearly evidences that signal contributions *B* and *C* of sample 2 belong to the same nuclei and represent the high- and low-frequency maxima of a signal broadened by the second-order contribution of quadrupole coupling.

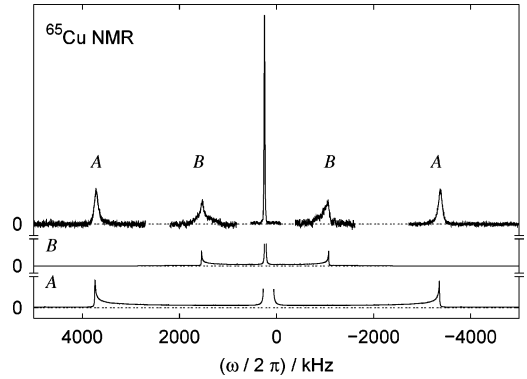

Figure 7. Top: ^{65}Cu NMR signal of an Al-rich $Cu_{1-x}Al_2$ sample 4 aligned in a magnetic field. The field used for the orientation of the crystallites was orthogonal to the external field of the measurement. The main transitions of signals *A* and *B* overlap for this orientation. The intensity of the satellites of signal *B* are increased. The spectrum is composed of five separately measured signals. Middle and bottom: Simulated ^{65}Cu NMR signals with $C_Q = 5.2$ MHz for *B* and $C_Q = 14.3$ MHz for *A* both with $\eta = 0$.

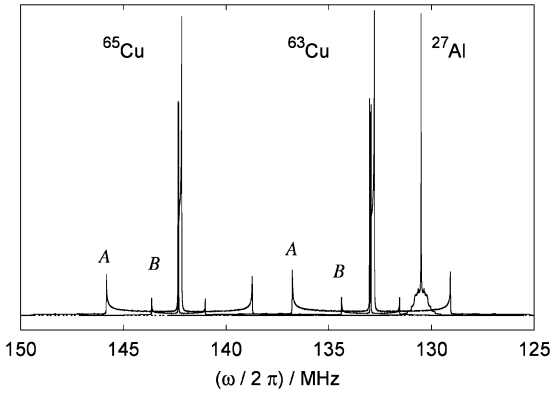

Figure 8. Simulated full NMR spectrum of $Cu_{1-x}Al_2$. The parameters used for the simulation are (*A*) $^{65}C_Q = 14.3$ MHz, $^{63}C_Q = 15.4$ MHz and (*B*) $^{65}C_Q = 5.2$ MHz, $^{63}C_Q = 5.6$ MHz all with $\eta = 0$ and $^{27}C_Q = 2.8$ MHz with $\eta = 0.41$. The spectra are scaled to the same value of maximum intensity.

The satellites of the signals were measured for $\theta \approx 90°$ in order to obtain independent information about the spectral parameters (Figure 7). The overlap of the ^{63}Cu and ^{27}Al signals (cf. Figure 8) was avoided by measuring the ^{65}Cu signal. The quadrupole coupling constants determined from the satellite positions are in good agreement with those determined from the frequency dependence of the main transition of sample 4 being a valuable proof of the axial symmetry of the electric field gradient.

From X-ray diffraction and from the orientation-dependent NMR measurements it can be concluded that the principal axis V_{ZZ} of the electric field gradient tensor as well as the direction of the largest absolute value of the magnetic susceptibility are parallel to the crystallographic *c* axis of $Cu_{1-x}Al_2$.

The larger line width of the satellites compared with the main transition indicates a narrow distribution of quadrupolar frequencies due to small variations in the orientations of the crystallites or atomic disorder. The increase of the satellite line width of signal *B* with respect to signal *A* refers to a higher degree of variations of the environment of the atoms corresponding to signal *B*. Nevertheless, the similarity of both

Cu positions can be seen in the Knight shifts of signals *A* and *B* being almost equal. Only a small shoulder is visible at high frequencies for $\theta \approx 0°$. Similar spin−lattice relaxation times T_1 at ambient temperature were observed for both signals: $T_1 = 2.7(1)$ ms for *A* and $T_1 = 3.7(3)$ ms for *B*. This is also the case for the spin−spin relaxation time $T_2 \approx 450\ \mu$s.

3.1.3. SEDOR Experiments. SEDOR is especially suited to investigate the local environments of the atoms.[21] The spectral intensity S_0 of an unperturbed echo experiment for spin **I** is compared with an perturbed echo experiment for spin **I** of spectral intensity *S*. The perturbation is achieved by excitation of a spin **S** resulting in a reduction of the echo intensity due to dipole−dipole coupling. The latter is sensitive to the inverse third power of the interatomic distance and depends on the orientation of the coupling vector with respect to the magnetic field of the measurement. The technique is robust concerning T_2 effects.[26]

The ratio of the spectral intensities S/S_0 can be calculated for interpulse durations τ and the angle θ between the vector r_{IS} joining the interacting nuclei and the applied magnetic field of the measurement using the second moments M_2^{IS} (refs 27 and 28):

$$\frac{\overbrace{\mathsf{I}_i(2\tau)}^{S}}{\mathsf{I}_0} = \frac{\overbrace{\mathsf{F}_i(2\tau)}^{S_0}}{\mathsf{F}_0}\, e^{\left(-2\tau^2 M_2^{IS}\right)} \qquad (1)$$

$$M_2^{IS} = \frac{4}{15}\left(\frac{\mu_0}{4\pi}\right)^2 \hbar^2 {\gamma_I}^2 {\gamma_S}^2 \mathbf{S}(\mathbf{S}+1)\sum \frac{(1-3\cos^2\theta)^2}{{r_{IS}}^6} \qquad (2)$$

The ratio S/S_0 for $\mathbf{I} = {}^{65}$Cu affected by dipole−dipole coupling to the $\mathbf{S} = {}^{27}$Al or $\mathbf{S} = {}^{63}$Cu signal was investigated in the heteronuclear ^{65}Cu−^{27}Al and ^{65}Cu−^{63}Cu experiments. The experiments were performed on the sample 4 aligned in a magnetic field for two reasons: the signals do not overlap, and, thus, they can be manipulated separately for certain orientations of the sample; the angular dependence of the dipolar interaction gives additional insights to the coupling. We used angles of $\theta \approx 22°$ and $\theta \approx 45°$ between the directions of the magnetic fields applied for alignment of the crystallites and the NMR measurements.

The observed ratio S/S_0 of the ^{65}Cu NMR signals *A* and *B* can be seen in Figure 9. The reduction for both signals reveals internuclear distances of the interacting particles in the order of a few angstroms. Thus, the Cu nuclei causing signals *A* and *B* belong to the same phase.

The intensity and angle dependence of the S/S_0 signals evidence different Cu and similar Al coordination for the Cu atoms of signal *A* and *B* by the ^{65}Cu−^{63}Cu and ^{65}Cu−^{27}Al experiments, respectively.

3.1.4. Second Moment Calculation. An exact calculation of the ratio S/S_0 cannot be performed on the basis of the present experiments: The duration of the pulses is too long to be neglected, and the width of the signals varies with the orientation of the sample resulting in a different amount of the excited spins for various sample orientations. Nevertheless, an analysis of the model and orientation-dependent second moment contains valuable information.

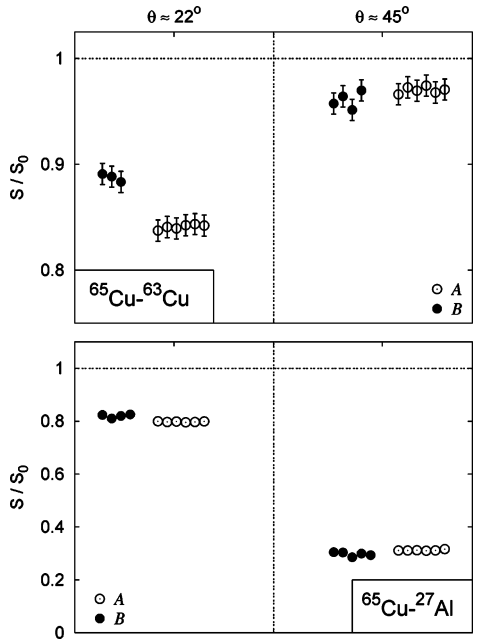

Figure 9. Ratio S/S_0 of the reduced spectral intensities *S* with respect to the full spectral intensity S_0 of the ^{65}Cu central transition measured by SEDOR. A constant interpulse delay of $\tau = 200\ \mu$s was used for two orientations of sample 4 aligned in a magnetic field (left, $\theta \approx 22°$, and right, $\theta \approx 45°$). Top, ^{65}Cu−^{63}Cu, and bottom, ^{65}Cu−^{27}Al heteronuclear experiments. Measurements of signal *A* are represented by empty and signal *B* by full symbols.

The calculations of the second moment are based on the crystal structure of $Cu_{1-x}Al_2$[12] and the various models of local order of the atoms. Furthermore, within model II we have considered Cu sites with one or two Cu vacancies in the neighborhood (II-1 and II-2, respectively).

The angular dependencies of M_2^{IS} for ^{65}Cu−^{63}Cu and ^{65}Cu−^{27}Al couplings are depicted in Figure 10. The calculated second moments increase for the different models with the number of interacting nuclei. As a result of the much higher natural abundance of ^{27}Al compared to ^{63}Cu, the ^{65}Cu−^{27}Al coupling is larger than the ^{65}Cu−^{63}Cu coupling. A minimum of M_2^{IS} for the ^{65}Cu−^{63}Cu interaction is calculated for the angle of $\theta = 56.25°$ between the vector joining the next neighbor Cu atoms and the magnetic field. For $\theta = 54.74°$ being the magic angle the dipole−dipole coupling of the ^{65}Cu to the next neighbor ^{63}Cu atoms becomes zero (cf. eq 2). The second moment of the ^{65}Cu−^{27}Al coupling has a maximum for this orientation due to the contributions of the Al atoms having angles between the coupling vectors and the magnetic field different from the magic angle.

3.1.5. Evaluation of a Structural Model from SEDOR Experiments. A model of the local ordering on the atomic scale in $Cu_{1-x}Al_2$ can be established combining the results of the second moment calculations and the SEDOR experiments.

Signal *A* represents Cu without neighboring vacancies or substitution of the atoms in the structure of $Cu_{1-x}Al_2$. The SEDOR decay of this signal serves therefore as a measure of the corresponding M_2^{IS} ($CuAl_2$). Models I and III can be

(26) Cull, T. S.; Joers, J. M.; Gullion, T.; Norberg, R. E.; Conradi, M. S. *J. Magn. Reson., Ser. A* **1998**, *133*, 352.
(27) Gee, B.; Eckert, H. *J. Phys. Chem.* **1996**, *100*, 3705.
(28) Van Vleck, J. H. *Phys. Rev.* **1948**, *74*, 1168.

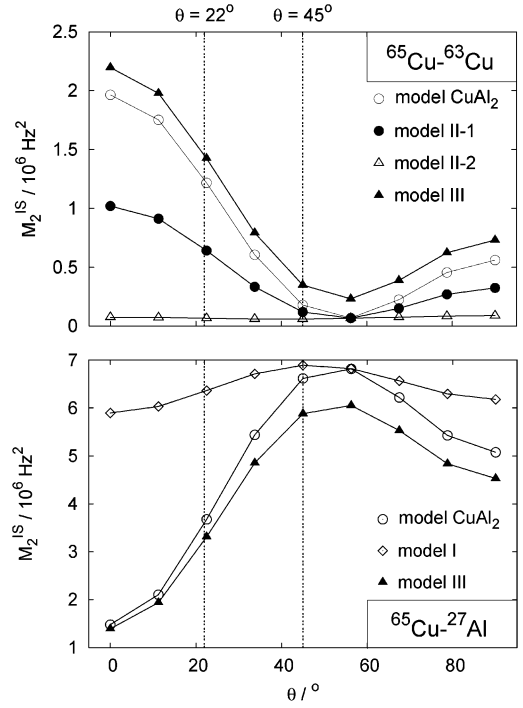

Figure 10. Calculated second moment M_2^{IS} for heteronuclear coupling. Top: ^{65}Cu−^{63}Cu with **I** = ^{65}Cu and **S** = ^{63}Cu. Bottom ^{65}Cu−^{27}Al with **I** = ^{65}Cu and **S** = ^{27}Al. Model $CuAl_2$ refers to Cu atoms having neither vacancies nor substitution of atoms in the environment. Defects and substitutions of the **S** spins of the other models are in the first coordination of the **I** spins. Models I and II and models II and $CuAl_2$ cannot be distinguished by the ^{65}Cu−^{63}Cu and ^{65}Cu−^{27}Al experiments, respectively. Full lines are a guide to the eye.

rejected due to the orientation dependence of the M_2^{IS} of ^{65}Cu−^{27}Al coupling (bottom in Figure 10, see also Table 1). This differs for models I and III from that of $CuAl_2$ being in contradiction to the observed equal SEDOR decays of signal *A* and *B* (Figure 9, bottom). In addition, model III can be ruled out by the orientation dependence of M_2^{IS} for ^{65}Cu−^{63}Cu coupling, which is similar for models III and $CuAl_2$ (Figure 10, top). According to SEDOR experiments, M_2^{IS} of the suited model is predicted to be equal for $\theta \approx 45°$ and smaller for $\theta \approx 22°$ than M_2^{IS} of $CuAl_2$ (Figure 9, top).

The remaining models II-1 and II-2 are supported by the results of the ^{65}Cu−^{63}Cu measurements and calculations. The smaller M_2^{IS} of model II-1 compared to M_2^{IS} of $CuAl_2$ for $\theta \approx 22°$ is in agreement with the observed SEDOR decays being larger for signal *A* than for signal *B*. However, the existence of Cu atoms with two neighboring Cu vacancies (model II-2) besides Cu atoms with only one neighboring Cu vacancy (model II-1) cannot be excluded. The observed angular dependence of the ^{65}Cu−^{63}Cu SEDOR decay indicates that the majority of the coupling is due to Cu atoms with only one neighboring vacancy (model II-1).

The model with Cu vacancies is in agreement with expectations from chemical bonding explaining the increase of the lattice parameters with increasing *x* in $Cu_{1-x}Al_2$. Because the copper atoms are participating in the three-center Cu−Al−Cu bond, the Cu vacancies result in the loss of attractive forces in all directions.[12] ^{27}Al NMR measurements served as a source of independent information about the influence of the Cu vacancies on the properties of the compound. These experiments were used as a check for consistency with the model derived from the Cu NMR measurements.

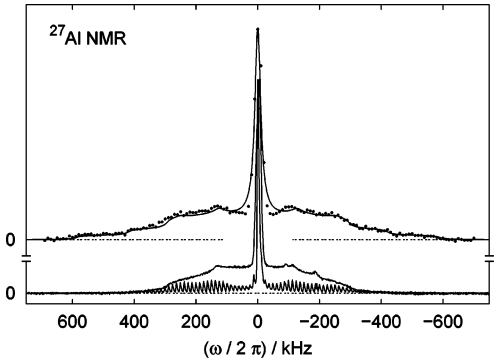

Figure 11. ^{27}Al NMR signal of Al-rich $Cu_{1-x}Al_2$ (sample 2). Top: Wide-line spectrum measured by selective excitation technique (points). The full line represents a calculated spectrum for $C_q = 2.8$ MHz and $\eta = 0.41$. Bottom: The full lines represent the wide-line spectrum and the MAS spectrum with pronounced rotational sidebands. The signals are normalized to the same value of maximum intensity, and the frequency scale is given relative to the used carrier frequency.

3.2. Aluminum NMR.

3.2.1. Line Shape and Parameters of the Spectrum. The ^{27}Al NMR spectrum measured by the selective excitation technique for sample 2 is depicted in Figure 11. The intensity of the outermost signal contributions of the 5/2 ↔ 3/2 and −5/2 ↔ −3/2 satellite transitions was too small for a separation from the background. Taking the parameters of Torgeson and Barnes[25] ($C_Q = 2.8$ MHz and $\eta = 0.41$), we find that the simulated signal is in good agreement with the experimental data but is in contradiction to the observations of Bastow and Celotto[18] who measured with a small number of different carrier frequencies ($C_Q = 4.87$ MHz and $\eta = 0.20$). The latter technique of building the envelope of a small number of wide-line signals gives only a very rough estimate of the parameters of the signal, especially for a non-axial symmetric coupling tensor. The Knight shift of the signal $K = 0.150(1)\%$ is in agreement with former results.[18,25] Torgeson and Barnes[25] observed a non-axial symmetric Knight shift with $K_X = 0.159(1)\%$, $K_Y = 0.153(2)\%$, and $K_Z = 0.148(10)\%$ by continuous wave technique while Bastow and Celotto[18] report an isotropic Knight shift of $K_{iso} = 0.148(1)\%$.

3.2.2. Aluminum Environment. The wide-line spectrum measured by the selective excitation technique covers a larger frequency range than the single echo spectrum of sample 2 measured with a MAS probe (Figure 11). This is due to the high quality factor of the MAS probe and the finite duration of the pulses, leading to systematic errors of the line shape. A comparison of the line shape of the central transition measured using the MAS probe with and without sample rotation is shown in Figure 12. The static spectrum shows a slightly asymmetric broadening which may be due to the small anisotropy of the Knight shift reported in the literature.[25] Using a rotation frequency of 12.5 kHz the signal width was reduced, and three shoulders at lower frequencies could be detected. These correspond to different environments of Al in $Cu_{1-x}Al_2$ caused by the Cu vacancies which may also be the origin of the asymmetric broadening of the static signal. In fully occupied $Cu_{1-x}Al_2$ each aluminum atom has four nearest copper ligands (Figure 1). Because of the

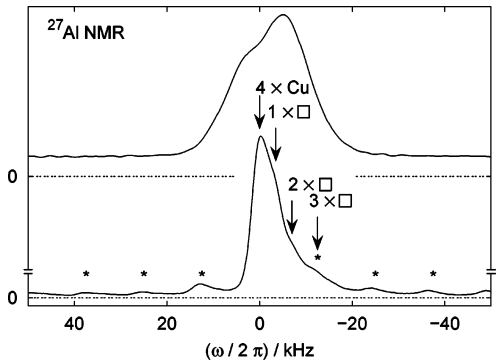

Figure 12. ^{27}Al NMR signal of Al-rich $Cu_{1-x}Al_2$ (sample 2). Wide-line spectrum (top) and MAS spectrum ($\nu_{rot} = 12.5$ kHz, bottom). The asterisks mark rotational side bands, while the arrows indicate shoulders in the signal. The intensities of both spectra are normalized to the same maximum value, and the frequency is given relative to the used carrier frequency.

generally small concentration of copper vacancies, all the local environments without and with one, two, three, or four vacancies are possible with decreasing probability. The four signals detected in the ^{27}Al NMR spectrum are therefore in good agreement with the number of possible local arrangements.

Table 1. NMR Experiments and their Results Concerning the Crystal Structure of $Cu_{1-x}Al_2$[a]

	$CuAl_2$	Model I	Model II-1	Model II-2	Model III
^{63}Cu and ^{65}Cu NMR	−	+	+	+	+
$\nu(\theta)$ ^{63}Cu NMR	−	+	+	+	+
SEDOR and $M_2^{IS}(\theta)$ $^{65}Cu-^{27}Al$		+			−
SEDOR and $M_2^{IS}(\theta)$ $^{65}Cu-^{63}Cu$	−		+	+	−
^{27}Al NMR	−	−	+	+	+

[a] The minus (−) indicates that the results are in contradiction to the model, and the plus (+) indicates that the results are in agreement with the model.

4. Conclusion

By combined application of different NMR techniques (Table 1) and calculations of the second moment M_2^{IS} we demonstrated the homogeneity range of $Cu_{1-x}Al_2$ to be realized by Cu vacancies. This finding is in agreement with the chemical bonding analysis and also explains the increase of the lattice parameter with increasing Cu deficiency. The Cu vacancies result in two different Cu signals and also influence the Al coordination leading to at least four overlapping signals with slightly different Knight shifts.

The two Cu signals with an intensity ratio of 1:24 originate from the nonequivalent environments of Cu atoms due to the Cu vacancies. The ^{63}Cu coupling constants of the axial symmetric electric field gradient are $C_Q = 5.6(1)$ MHz and $C_Q = 15.4(1)$ MHz for Cu atoms with and without vicinal Cu vacancies, respectively. The influence of the Cu−Cu bonding interaction on the electric field gradient may be observed in the smaller field gradient for the Cu atoms with neighboring Cu vacancies. On the basis of our NMR experiments other models explaining the non-stoichiometric composition of $Cu_{1-x}Al_2$ discussed in the literature can be ruled out by the measurements of the angular dependence of the heteronuclear dipole−dipole coupling.

Acknowledgment. We are grateful to Andreas Leithe-Jasper for preparation of the single crystal and to Raul Cardoso-Gil for X-ray diffraction measurements. Furthermore, we thank Jürgen Haase, Andrei Gippius, and Jan Hildebrandt for stimulating discussions.

CM062313K